Small Landslide Susceptibility and Hazard Assessment Based on Airborne Lidar Data

Omar E. Mora, Jung-kuan Liu, M. Gabriela Lenzano, Charles K. Toth, and Dorota A. Grejner-Brzezinska

Abstract
Landslides are natural disasters that cause environmental and infrastructure damage worldwide. To prevent future risk posed by such events, effective methods to detect and map their hazards are needed. Traditional landslide susceptibility mapping techniques, based on field inspection, aerial photograph interpretation, and contour map analysis are often subjective, tedious, difficult to implement, and may not have the spatial resolution and temporal frequency necessary to map small slides, which is the focus of this investigation. We present a methodology that is based on a Support Vector Machine (SVM) that utilizes a lidar-derived Digital Elevation Model (DEM) to quantify and map the topographic signatures of landslides. The algorithm employs several geomorphological features to calibrate the model and delineate between landslide and stable terrain. To evaluate the performance of the proposed algorithm, a road corridor in Zanesville, Ohio, was used for testing. The resulting landslide susceptibility map was validated to correctly identify 67 of the 80 mapped landslides in the independently compiled landslide inventory map of the area. These results suggest that the proposed landslide surface feature extraction method and airborne lidar data can be used as efficient tools for small landslide susceptibility and hazard mapping.

Introduction
The hazards of natural disasters occur from processes of the earth and cause damage, devastations, loss of life, and environmental change. One particular natural hazard of interest known to cause economic, human and environmental damage worldwide are landslides (Glenn *et al.*, 2006). Landslides have consistently damaged human infrastructure and have impeded the daily lives of many. They have a broad range of geologic processes that cause the downward movement of mass over spatial and temporal scales (McKean and Roering, 2004). In addition, their effects have a strong dependability on their spatial pattern of incident, rate of recurrence, and amount of movement (McKean and Roering, 2004). Their hazards are well-understood, yet current methods of identifying and assessing their conditions are inefficient, and are

difficult to predict. Existing techniques are typically based on field inspection, aerial photograph interpretation, and contour map analysis (Booth *et al.*, 2009). However, these methods have limitations that reduce the accuracy, completeness and reliability necessary to map landslides with high probability, especially, small failures where mass movement rates are slower (Booth *et al.*, 2009; Galli *et al.*, 2008). Additionally, many sites are not easily accessed for field inspections. Highly vegetated areas present difficulties for both on-site inspections and aerial photographic interpretation. Historical contour maps do not have the resolution necessary to map small landslides in highly vegetated areas where conventional remote-sensing methods cannot penetrate the land cover (Van Den Eeckhaut *et al.*, 2005; Booth *et al.*, 2009; James *et al.*, 2012). For these reasons, traditional methods are not cost-effective and a new approach to landslide susceptibility and hazard mapping is necessary.

Remote-sensing technology has seen large advances in the past decade, in cost, accuracy, and accessibility. One of the major improvements has been the spatial resolution of Light Detection and Ranging (lidar) technology. In earlier stages only coarse nominal point spacing (>10 meters) was available. Improvement of this technology has allowed for higher spatial resolutions (<1 meter). The increase made in spatial resolution provides mapping opportunities at remarkable scales. This tool provides the accuracy necessary to map surface models precisely (Shan and Toth, 2008; Jaboyedoff *et al.*, 2012). Furthermore, it has the potential to overcome many challenges faced in landslide susceptibility mapping, for example, the spatial resolution, broad terrain coverage and accuracy necessary to map precise surface models. A particular lidar technology capable of overcoming the aforementioned challenges is airborne lidar. This instrument is capable of penetrating vegetation, mapping areas up to thousands of square kilometers (Shan and Toth, 2008; Guzzetti *et al.*, 2012), and providing sub-meter spatial resolutions. For these reasons, it is a prime consideration.

Previous landslide susceptibility mapping techniques revealed the potential that remote-sensing technology presented to identify and map the geomorphic features related to landslide morphology (McKean and Roering, 2004; Glenn *et al.*, 2006; Booth *et al.*, 2009). However, their focus has been on mapping large landslides in hilly terrain and mountainous regions, along coastal bluffs, and river basins (e.g., Van Den Eeckhaut *et al.*, 2005; Booth *et al.*, 2009; Ballabio and Sterlacchini, 2012; Tien Bui *et al.*, 2012). Less attention has been paid to map small failures, which impact our transportation networks. Small failures have been overlooked in previous

Omar E. Mora, Charles K. Toth, and Dorota A. Grejner-Brzezinska are with the Department of Civil, Environmental and Geodetic Engineering, The Ohio State University, 470 Hitchcock Hall, 2070 Neil Ave., Columbus, OH 43210 (mora.30@osu.edu).

Jung-kuan Liu was with the Department of Civil, Environmental and Geodetic Engineering, The Ohio State University, Columbus, OH 43210, and currently with the CSS-Dynamac/National Operations Center, Bureau of Land Management, Denver Federal Center, Building 50, Denver, CO 80225.

M. Gabriela Lenzano is with the International Center of Earth Sciences (ICES), UNCuyo-CONICET, Ciudad Universitaria, Mendoza, Argentina.

studies, potentially due to their impact being less severe compared to large landslides. Furthermore, the spatial resolution needs to be relevant to the scale of the morphological features of the landslides in order to understand the spatial and temporal process evident in small landslide morphology (Glenn *et al.*, 2006). To our best knowledge, small landslide susceptibility mapping has not been addressed in the literature and an evaluation is necessary to understand and propose a means of hazard assessment for the prevention of future events.

This paper presents a novel approach for small landslide susceptibility mapping utilizing an airborne lidar-derived Digital Elevation Model (DEM). The approach employs several geomorphologic features to analyze the local topography, specifically: the direction cosine eigenvalue ratios (λ_1/λ_2 and λ_1/λ_3), resultant length of orientation vectors, aspect, roughness, hillshade, slope, a customized Sobel operator, and soil type. A sample set extracted from the data is used as observations of landslide and stable terrain to calibrate the supervised classification algorithm of Support Vector Machine (SVM). The calibrated SVM model is subsequently used to classify the lidar-derived DEM based on the extracted surface features. Then, as a post-classification step, flat terrain is filtered and classified as stable terrain. Consequently, a conditional dilation/erosion filter is applied to minimize misclassified locations by the SVM algorithm, in addition to suppressing noise and generating landslide susceptible regions (clusters). Landslide susceptible regions are then analyzed to map areas of potential landslide activity. Finally, in order to evaluate the performance of our proposed approach, we assess how well the algorithms mapped landslides match the reference inventory mapped landslides.

Study Area and Data

Study Area
The study area selected was along the transportation corridor of state route (SR) 666 in Zanesville, Ohio, located in north-central Muskingum County (Approx. Latitude: N39° 58' 00", Longitude: W81° 59' 00") along the east side of the Muskingum River. The study area begins at the intersection of SR-60 within the City of Zanesville just north of Interstate 70 (I-70)

and south of the Muskingum River at mile marker (MM) 0.00, and ends at the intersection with SR-208 east of the Village of Dresden at MM 14.34 (23 km). The extent of the project coverage is 23 kilometers in length along SR-666 with a varying width of 75 to 180 meters and approximately 3.0 km². The area is characterized by high vegetation densities, stream and river channeling, and some residential development. The study area was chosen due to the availability of an airborne lidar-derived DEM, a detailed landslide inventory map, and its prolonged history of slope instabilities, especially in areas where the river is close to the roadway. In 2004 and 2005, Muskingum County was declared a National Disaster Area due to extensive flooding in both tributaries and the main river channel. Along the road seven separate sections damaged by landslides were corrected as a result of these storm events. Figure 1 presents an overview map of the study area.

Data
The lidar data was acquired in the spring of 2012 and has a point density of 5 pts/m². The vertical accuracy of the points was assessed after the lidar was adjusted to the hard surface control. The vertical accuracy of the points was assessed by the root mean square error (RMSE), which was 9 cm for soft surfaces and 5 cm for hard surfaces. Additionally, the vertical accuracy was evaluated by the standard deviation, which was 6 cm and 5 cm for soft and hard surfaces, respectively. The bare earth, filtered from the lidar data, was subsequently used for this investigation. The lidar point cloud was bare earth filtered, and then was interpolated to a spatial resolution of 50 cm using Kriging, after evaluating the nominal point spacing to be 45 cm. The statistical results demonstrated that Kriging provided the minimum error between the interpolated surface (DEM) and the bare-earth filtered lidar point cloud. For this reason, it was selected as the prime interpolation method. The preprocessing of the bare earth lidar data, including converting to a regular grid, was done using LAStools (Isenburg, 2013) and ArcGIS®, respectively. All sequential processing was performed in MATLAB. The results of the processing steps were integrated into the project GIS database.

For the project area a geo-hazard inventory and evaluation of mass movement affecting the transportation network was completed in 2006 by the Ohio Department of Transportation
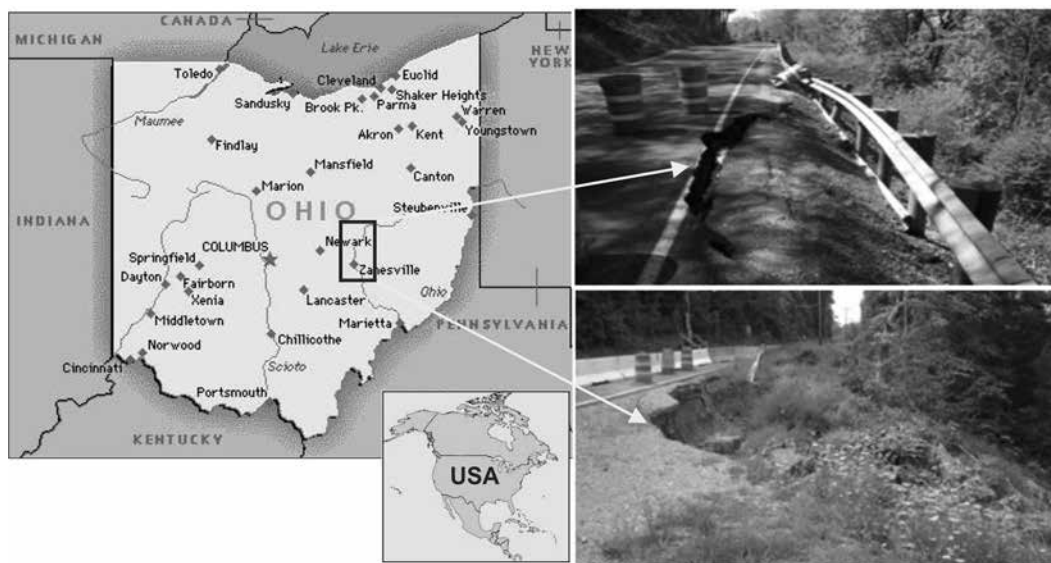

Figure 1. Study area along transportation corridor SR-666, north of Zanesville, Ohio. The figures on the right display examples of rotational slides affecting the embankment, near mile marker 7.3 (top), and 1.47 (bottom) that have since been stabilized.

(ODOT) Office of Geotechnical Engineering, and provided important information about the general locations of landslides affecting the road prism. An updated landslide inventory map was compiled by a team of experts from Kent State University and The Ohio State University through contour map analysis, geo-hazard inventory evaluation and on-site validation in the summer of 2012. The updated landslide inventory was used for the investigation. Typical landslides affecting the road prism are: rotational, translational, complex, rockfall debris, and mudslides. The slopes for areas of instability range from 18° to 80°, in which the most frequently slope observed was 45°; additionally, the landslides described have a range of ages per the historical documents. The importance of the inventory map is that it provides a reference against which we can evaluate the performance of our proposed approach. A limitation found in the reference map is that it only provides the extents of the mapped landslides and does not offer additional information about the rate of change experienced. The mapped landslides provided in the inventory range from 200 m^2 to 27,000 m^2 in area. The soil map used for this study was available online from the Ohio Department of Natural Resources (ODNR) website (*http://www.dnr.state.oh.us/tabid/9051/Default.aspx*).

Methodology

The effects of mass movement are important and greatly dependent on their spatial pattern of occurrence, frequency, and amount of activity (McKean and Roering, 2004). The temporal processes of landslides can reveal a wealth of information regarding the magnitude of surface deformation experienced and the expected change over time. While temporal changes cannot be revealed from individual surface models, identifying landslide-specific spatial features from single surface models is important, as not all the changes detected by temporal analysis represent landslide suspect areas. This study is focused on examining and evaluating single surface models, and the developed method can serve as a tool to filter landslide suspect areas. Landslides are known to have rougher surfaces than neighboring stable terrain. This is due to the mechanics, subsidence, and surface deformation experienced. The surface roughness of landslide (bottom) terrain experiences higher topographic variability than stable (top) terrain as illustrated in Figure 2. McKean and Roering
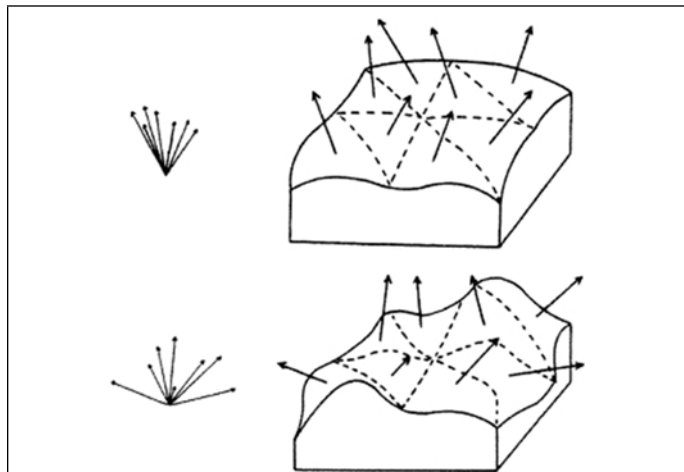

Figure 2. The figure illustrates surface normals representing topographic variability (roughness) in a DEM. Smooth terrain (top), illustrates less variation. Rough terrain (bottom), illustrates higher variability from McKean and Roering, 2004.

(2004) and Glenn *et al.* (2006) exploited the surface roughness to detect and map landslides, and confirmed that the surfaces of landslides are rougher than neighboring stable terrain. For these reasons, the surface roughness will be the focus of the proposed algorithm.

The objective of the approach is to identify surface features indicative of landslide activity and map their locations in the study area. The process to identify landslide surface features is as follows: (a) filter airborne lidar point cloud to contain bare-earth points only, (b) rasterize the bare-earth point cloud using Kriging interpolation method, (c) perform surface feature extraction, (d) classify lidar-derived DEM, (e) perform post-classification filtering, and lastly (f) map areas experiencing landslide activity. The feature extraction algorithms used are described in the following sections.

Feature Extraction

To extract and quantify the amount of surface roughness observed in the terrain, the following eight geomorphological features were utilized: aspect, hillshade, roughness, slope, eigenvalue ratios (λ_1/λ_2 and λ_1/λ_3), customized Sobel operator, and the resultant length of orientation vectors. The selected feature extraction methods are further discussed below. Some of the surface feature extraction methods selected have been used to expose various topographic patterns (e.g., McKean and Roering, 2004; Glenn *et al.*, 2006) and were therefore prime considerations. The standard algorithms available in the MATLAB TopoToolbox by Schwanghart and Kuhn (2010) were used for the evaluation of aspect, hillshade, roughness, and slope. Fixed sampling windows of size (9 × 9) were used to evaluate the direction cosine eigenvalue ratios and length of orientation vectors. Furthermore, a statistic measure of the standard deviation is evaluated from small sampling windows of a fixed size (9 × 9) to define the local topographic variability of aspect, hillshade, roughness, slope, resultant length of orientation vectors, and customized Sobel operator. Areas experiencing higher degrees of surface deformation will illustrate higher topographic variability, thus, delineating rough and smooth terrain.

Aspect
Slope orientation is the compass direction a land surface faces. To evaluate the slope orientation, also known as aspect, for a DEM grid point of a (3×3) local neighborhood, Z_{11}, shown in Equation 1, the surface normals need to be computed. Subsequently, the mapping system needs to be converted from a two-dimensional Cartesian coordinate system to a polar coordinate system: $\theta = arctan\left(\dfrac{N_x}{N_y}\right)$, where, θ is the angle in the polar coordinate system, and N_x and N_y are the surface normals in the east-west and north-south direction, respectively. Finally, the slope orientation of a cell can be computed:

$ASPECT = \dfrac{\theta}{\pi} * 180° + 180°.$

$$\begin{bmatrix} Z_{02} & Z_{12} & Z_{22} \\ Z_{01} & Z_{11} & Z_{21} \\ Z_{00} & Z_{10} & Z_{20} \end{bmatrix} \tag{1}$$

Hillshade
The relief depiction of a grid point in a DEM is described by the lighting effect of the angle between the surface and the incoming light beam. The approach uses the illumination

from a single direction for the shading of the terrain relief. Hillshading is typically used to display shaded relief images, however, it was observed that this feature provided important information regarding topographic variability found in landslide morphology, for this reason, hillshading was included. The shaded relief images used throughout this paper and surface feature extractor follow the approach described in Katzil and Doytsher (2003).

Roughness

The metric used to quantify deviations of a surface is called roughness. If the deviations are small, the surface is considered to be smooth, and if the deviations are high, it is considered rough. Roughness can be evaluated by computing the largest inter-cell difference of a central pixel and its surrounding cells using Equation 1, $R = Max(Z_{ij} - Z_{11})$, where $i = 0\text{-}2$, $j = 0\text{-}2$.

Slope

The maximum rate of change between a cell and its neighbors is known as slope. It is evaluated by computing the steepest descent of a DEM using Equation 1, $S_{D8} = max\left[\dfrac{Z_{ij} - Z_{11}}{h\phi(ij)}\right]$ m

$i = 0\text{-}2$, $j = 0\text{-}2$. Where $\phi(ij) = 1$ for the cardinal (north, south, east, and west) and $\phi(ij) = \sqrt{2}$ for the diagonal neighbors.

Direction Cosine Eigenvalue Ratios

The eigenvalue ratios express the amount of roughness in three-dimensional surfaces (Kasai *et al.*, 2009). The vectors are defined by their direction cosines: $x_i = sin\theta_i cos\phi_i$, $y_i = sin\theta_i sin\phi_i$ and $z_i = cos\theta_i$, where θ_i is the colatitude, and ϕ_i is the longitude of a unit orientation vector as described in McKean and Roering (2004). When considering $(x_1, y_1, z_1)\dots (x_n, y_n, z_n)$ as a set of n unit vectors perpendicular to each cell in the DEM, the orientation matrix, T, may be constructed, see Equation 2. Next, the eigenvalues are computed for T, consequently, $ln(\lambda_1/\lambda_2)$ and $ln(\lambda_1/\lambda_3)$ are evaluated, where, λ_k is the eigenvalue for $k = 1,2,3$. The ratios of normalized eigenvalues are often not normally distributed; for this reason, the logarithms of the ratios are evaluated (McKean and Roering, 2004). Lower eigenvalue ratios indicate that the unit orientation vector of the cells will have higher degrees of surface roughness (Woodcock, 1977; McKean and Roering, 2004).

$$T = \begin{bmatrix} \sum x_i^2 & \sum x_i y_i & \sum x_i z_i \\ \sum y_i x_i & \sum y_i^2 & \sum y_i z_i \\ \sum z_i x_i & \sum z_i y_i & \sum z_i^2 \end{bmatrix} \quad (2)$$

Resultant Length of Orientation Vectors

Another way to evaluate topographic variability is by computing the resultant length of orientation vectors in three dimensions in a sampling window from the direction cosines used to compute the eigenvalue ratios as illustrated in McKean and Roering (2004), $RL = ((\sum x_i)^2 + (\sum y_i)^2 + (\sum z_i)^2)^{1/2}$, where RL is the resultant length of orientation vectors. This measure can be used to define surface roughness as variations within local neighborhoods will be coincident for smooth topography, and greater variations will be displayed for rough topography (McKean and Roering, 2004).

Customized Sobel Operator

The Sobel operator computes an approximation of the gradient of the image intensity function. At each point in the image, the result of the Sobel operator is defined as either the corresponding gradient vector or the norm of this vector. The Sobel operator is based on convolving the image with a small and separable filter usually in a horizontal and vertical direction (Gonzalez and Woods, 2002).

Various kernels were evaluated, yet none of those tested

provided unique characteristics depicting landslide morphology. However, the kernels selected did extract distinctive features, thus, enhancing those found in landslides. The kernels of the connected neighborhood cells are as follows:

(A)

(B)

(C)

(D)

(3)

The kernels used to compute the gradients in horizontal $(\hat{G}_x)$, vertical $(\hat{G}_y)$, diagonal left $(\hat{G}_{dl})$, and diagonal right $(\hat{G}_{dr})$ directions are illustrated in Eq.uation (3A), (3B), (3C), and (3D), respectively. The magnitude of the gradient was computed by modifying the typically used form illustrated in Gonzalez and Woods (2002) to include all directions:

$$\hat{G} = \sqrt{\hat{G}_x^{\,2} + \hat{G}_y^{\,2} + \hat{G}_{dl}^{\,2} + \hat{G}_{dr}^{\,2}} \quad (4)$$

Soil Types

Soils have been widely considered in landslide susceptibility mapping studies (e.g., Wieczorek *et al.*, 1996; Gomez and Kavzoglu, 2005). The six primary soil types found within the study area consists of alluvium, glacial outwash, lacustrine soils, colluvium, residual soils, and manmade fill. Berks-Westmoreland complex (Bkf) soil found in 40 to 70 percent slopes was the soil type for approximately 92 percent of the mapped landslides in our study area, and was considered highly susceptible to landslides compared to all other soil types. Bkf has the most rugged terrain in the county and it is common to see unstable slopes in this soil type, in addition, the soil has a severe hazard of erosion. Moreover, cuts made along these slopes are unstable for building sites (Steiger, 1996). For these reasons, the underlying soil was considered an important surface feature to map landslides.

Landslide Classification

Extracting landslide surface features is the core step in landslide susceptibility mapping. To quantify topographic roughness it is necessary to understand and delineate the characteristics found in landslide morphology. Therefore, a sample set representing these distinct features is necessary. SVM is a supervised classification method that is well established, and known to produce acceptable results in landslide susceptibility mapping (Samui, 2008; Yao, *et al.*, 2008; Marjanovi , *et al.*, 2011; Micheletti, *et al.*, 2011; Ballabio and Sterlacchini, 2012; Tien Bui *et al.*, 2012). The objective is to classify the lidar-derived DEM based on the extracted surface features. In order

to automatically map terrain with surface features indicative of landslide activity, we analyze the surface features extracted as single observations with nine dimensions (surface features described earlier) to determine if the observation is representative of landslide activity for each cell in the DEM. If it is, then it is mapped as landslide susceptible, otherwise, it is mapped as stable. Each cell in the DEM is considered a nine-dimensional observation.

Support Vector Machine

SVM was developed by Vladimir Vapnik (1995). The idea of SVM is to determine the optimal hyperplane for linearly separable patterns (see Figure 3). If the patterns are not linear then, the data is projected into a higher dimensional space using a kernel. Support vectors are selected to delineate the two classes and maximize the margin between them. Support vectors in general are the most difficult data points to classify, thus, lying closest to the decision surface (Tien Bui *et al.*, 2012).

SVM was chosen for its advantages which are: its effectiveness in high dimensional spaces, it utilizes a subset of the training sample in the decision function (support vectors), various kernel functions may be applied for the decision function, and it works well when there is a small sample available for training. For these reasons, it was the prime consideration for classification. In general, the SVM algorithm is calibrated through a sample set of two classes enclosing all features desired. The two classes are landslide and stable terrain, and the aforementioned surface features are those used in our case. After calibration is complete, the algorithm is tested on an independent data set to evaluate its performance, a lidar-derived DEM in our case.

Flat Terrain Filtering

Landslides have shown to occur more often on steeper slopes (Gomez and Kavzoglu, 2005). Locations are safer in terms of potential failures where the slope is near flat. Therefore, as the slope increases so does the probability of failure. Table 1 illustrates unstable slopes for various types of mass movement taken from Soeters and van Westen (1996).

Given the ranges of slope instabilities in Table 1 and those found in our study area, it was determined that slopes (15° ≥) would be stable.
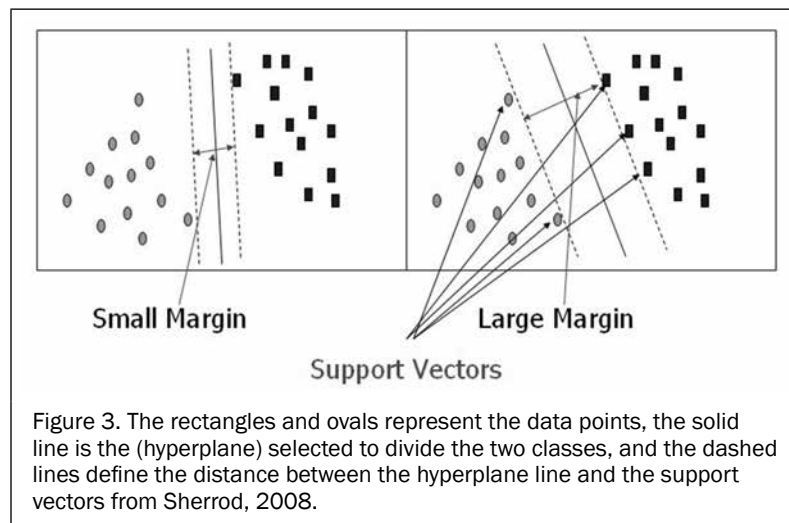
Conditional Dilation/Erosion Filter

Mathematical morphology is a method used to extract useful features found within an image that characterize shapes of objects (Gonzalez and Woods, 2002). Furthermore, it is helpful in filtering, which is our interest. Two common morphological operations are dilation and erosion. Dilation expands the shapes found within an image, while erosion removes them; both draw conclusions from a given structuring element (e.g., kernel). In our algorithm we used a conditional dilation/erosion filter as we wanted the components to satisfy a size threshold (Shapiro and Stockman, 2000). The filter was designed as a sliding window of size $n \times n$ (n must be an odd integer), with a given threshold, to determine if the center cell should be dilated or eroded, with respect to the local neighborhood, see Equation 5:

$$\frac{\# \, of \, failed \, cells}{\# \, of \, total \, cells \, in \, window} \geq Threshold \qquad (5)$$

The effect of the window size and threshold were tested and evaluated by having varying window widths between 3 and 21 cells and varying thresholds between 50 percent and 100 percent. After assessing potential thresholds, the most suitable window size and threshold found was 11 × 11 (5 m × 5m) and 60 percent, respectively. This particular window size and threshold did not distort the information produced from the classification algorithm. It only dilated and eroded the classification results as intended. For these reasons, the threshold and window size selected were subsequently used.

Noise Suppression

The analysis of clusters is a vital component of feature extraction. The importance of this step is to analyze clusters and suppress noise. Small regions do not provide useful information; therefore, they are not of interest and are ignored. The importance of determining a good threshold is so that the noise level is minimized and useful information is not lost. In our approach clusters of cells classified as landslide terrain are analyzed and evaluated to determine if the cluster will be classified as landslide or stable given the following criterion:

$$Cluster \, Area \geq Minimum \, Area \, Threshold \qquad (6)$$

The minimum area to be considered landslide susceptible was tested and evaluated by having varying areas of 50 to 250 m². This range was selected after evaluating the minimum size of the mapped landslides provided by the reference inventory map, which was 200 m². After evaluating potential thresholds, it was determined that 150 m², was the most appropriate threshold, for this reason, all clusters less than 150 m² were ignored and considered as noise. The criterion selected will allow for clusters of said size to be mapped as landslide susceptible, additionally, minimizing the probability of small landslides being overlooked.

TABLE 1. SLOPE INSTABILITY FOR MASS MOVEMENT TYPE

Mass Movement Type	Slope Instability
Fall and Topple	20 °- 30°
Rotational Slide	20° - 40°
Lateral Spread	< 10°
Mudslide	15° - 25°
Earth flow	> 25°
Debris avalanche	> 35°

Figure 3. The rectangles and ovals represent the data points, the solid line is the (hyperplane) selected to divide the two classes, and the dashed lines define the distance between the hyperplane line and the support vectors from Sherrod, 2008.
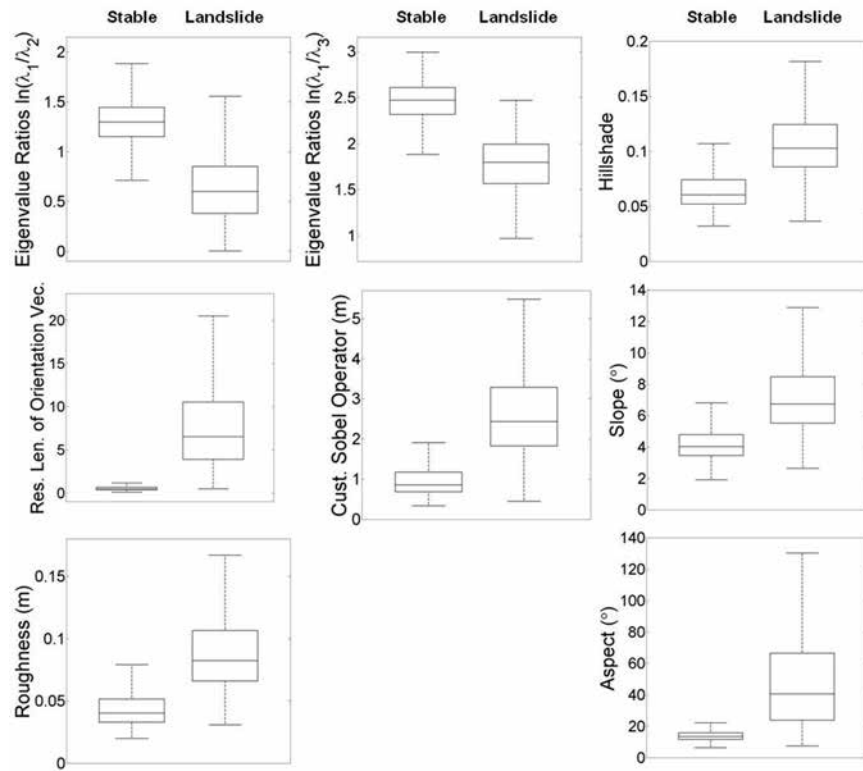
Figure 5. Distribution of training samples before being normalized between [-1 1], where, stable and landslide terrain are represented on the left and right, respectively, for each surface feature extracted.

Results

Training Sample Evaluation

To determine characteristics of landslide surface features in the study area, we first select a representative patch of a mapped landslide and stable terrain. We use a section 450 m north of MM9 as representative patches (see Figure 4). The size of the representative patch was 30 × 40 m (1,200 observations) for stable and 60 × 25 m (1,500 observations) for landslide terrain. The representative terrain elected was less than 1 percent of the entire study area. Next, we compute the surface features for each patch of terrain. Figure 5 shows the distribution of the samples elected for each surface feature. The topographic variability is higher for landslide than stable terrain. These patterns indicate that the landslide surface in our study area tends to experience higher amounts of surface deformation, meaning, it is rougher in texture. Earth processes that can generate such behavior are those of mass movement found in landslides.

The distributions in Figure 5 can be described as follows: the central mark in each box is the median (Q_2), the limits of the box are the 25th (Q_1) and 75th (Q_3) percentiles of the samples, the interquartile range (IQR) is equal to $Q_3 - Q_1$, the dashed line (whiskers) extend to the typically used Q_1 - 1.5(IQR) and Q_3 + 1.5(IQR) range which is about ±2.7 and 99.3 percent of the data, if the data are normally distributed. The remaining samples not lying within these limits are considered outliers (are not plotted). It is expected to observe outliers as not all landslide and stable terrain will have complete coverage of surface features representative of each. Therefore, it is possible to observe a few instances of landslide surface features in stable terrain and vice versa. These instances can be caused by noise in the data or irregularities observed within the terrain.

The representative patches demonstrate that 75 percent or more of the training samples are linearly separable for all surface features (see Figure 5). It was found that the eigenvalues ratio (see Table 2) express the behavior described in Mckean and Roering (2004), where the ratios are lower for landslide than stable terrain. Additionally, roughness, customized Sobel operator, aspect, hillshade, slope, and resultant length of orientation vectors, all experienced higher topographic variability (see Table 2) for landslide terrain as described in McKean and Roering (2004), and Glenn *et al.*, (2006). The variation of the surface features extracted is less for stable terrain for all surface features (Figure 5). This behavior is expected as stable terrain will experience lower rates of mass movement, therefore, most stable surface features are expected to express the same behavior.

Classification Performance Evaluation

The mapped locations will vary for each area, which reflects the variation in the topography (see Figure 6A, 6B, 6C, and 6D). Areas that are smooth will go undetected by the proposed algorithm (SW corner Figure 6B, and West section of Figure 6C), while areas that are rough will be mapped as landslide susceptible (East section of Figure 6A, and Figure 6B). The rough areas shown in Figure 6 tend to correspond to those mapped in Figure 7. Additionally, the areas identified as landslide susceptible by the proposed algorithm tend to coincide to those mapped locations provided by the reference inventory map, verifying that the proposed SVM model can delineate landslide terrain (see Figure 7).

In our study area, the proposed algorithm is capable of identifying 84 percent of the inventory map landslides (Figure 7A, 7B, 7C, and 7D). This defines that the training samples elected for calibrating the classification model were representative of the landslide terrain throughout the study area, thus, identifying a high percentage of the landslides. As anticipated earlier, some topographic features display characteristics of stable terrain within a landslide and vice versa. In particular (Figure 7D), a vast majority of the inventory mapped landslides are incorrectly
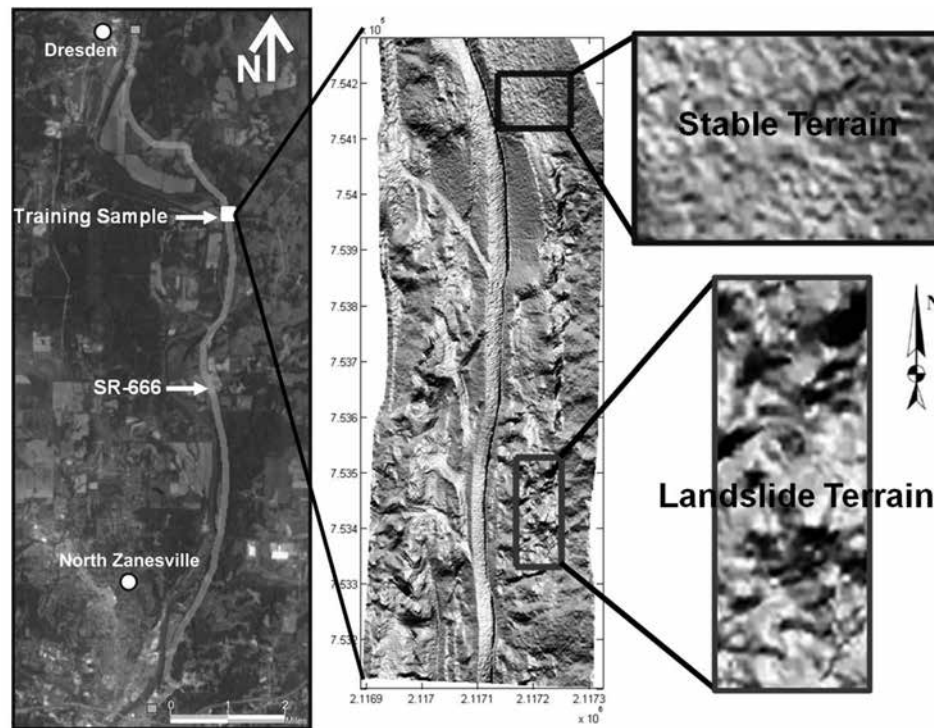
Figure 4. Lidar-derived hillshade map of SR-666, Zanesville, Ohio study area with the entire training sample used to calibrate the SVM algorithm outlined on top, and bottom, for stable and landslide terrain, respectively. The map is displayed in US survey feet for the State Plane Coordinate System, Ohio South Zone.

classified as stable, it is expected to classify incorrectly as the surface roughness is low for this area (see Figure 6D). In order to understand and potentially overcome the limitations further evaluation is necessary beyond the scope of this study.

The algorithm tends to misclassify topographic features with sharp edges or abrupt changes in elevation (SE and NE corner of Figure 7C and SE corner of Figure 7A). Even though, some of the incorrectly classified areas are along these abrupt surface changes, many inventory mapped landslides are also along abrupt changes in elevation, especially, along SR-666. Additionally, natural surface features also express abrupt changes or high surface roughness in the terrain, which include: riverbanks (SW corner of Figure 7C, and Figure 6C), bluffs, streams, creeks, and high elevation changes in a short distance. These natural features increase in surface roughness due to erosion and geomorphological events, which cause surface features to mimic those of landslides. Nonetheless, the algorithm also tends to overlook topographic features found within the boundaries of inventory mapped landslides due to insufficient surface roughness or man-made improvements

made to the environment. Although, a GIS database was available and can be used to minimize misclassifications generated by the proposed algorithm, it was only used to store geographic information of roads, rivers, creeks, residential development, etc, and the results generated by the algorithm.

In the study area, landslides have a range of ages and activity levels, so the surfaces of various landslides have undergone different degrees of surface deformation and post-failure improvement. The transportation of soil and weathering over time along older slides will cause them to smoothen and make them difficult to identify. For example, most of the mapped landslides shown in Figure 7D are mapped incorrectly due to the smooth topography from an older landslide. The removal of landslide features prevents the algorithm from detecting and identifying the mapped landslides in this area.

The performance of the proposed algorithm assessed how well the mapped areas coincide with the mapped landslides (reference) in the study area. The proposed algorithm was able to map a total of 200 locations throughout the study area. One hundred and ten of those identified areas overlapped mapped

TABLE 2. PERCENTILES OF DISTRIBUTION SAMPLES

|	Stable			Landslide		
Surface Feature	Q_1	Q_2	Q_3	Q_1	Q_2	Q_3
Eigenvalues Ratio $\ln(\lambda_1/\lambda_2)$	1.15	1.30	1.45	0.38	0.60	0.85
Eigenvalues Ratio $\ln(\lambda_1/\lambda_3)$	2.32	2.47	2.61	1.57	1.80	1.99
Roughness (m)	0.03	0.04	0.05	0.07	0.08	0.11
Customized Sobel Operator (m)	0.68	0.85	1.17	1.82	2.43	3.29
Aspect (°)	11.53	13.42	15.75	23.76	40.57	66.51
Hillshade	0.05	0.06	0.07	0.09	0.10	0.12
Slope (°)	3.45	4.02	4.79	5.51	6.74	8.47
Resultant Length of Orientation Vectors	0.35	0.49	0.69	3.91	6.54	10.56
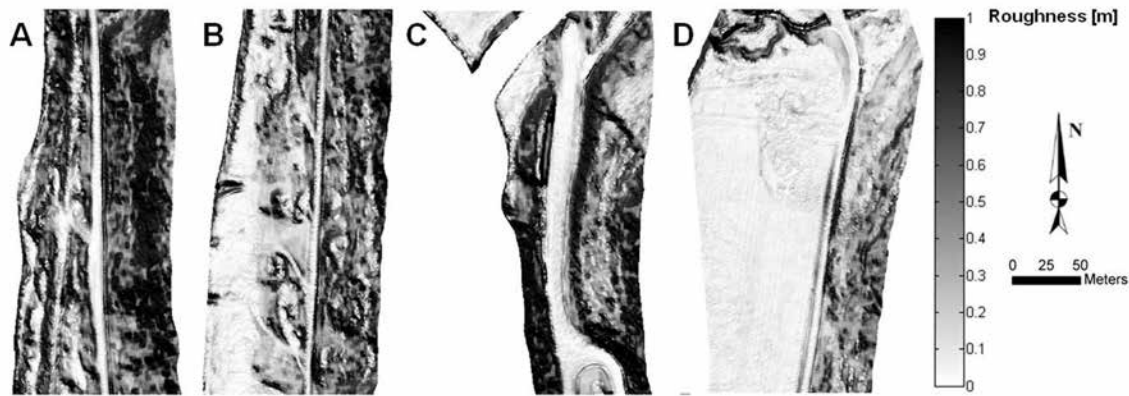
Figure 6. Topographic variability of four segments along SR-666. The surface feature used to depict the topographic variability was roughness. The higher variability the rougher the surface, which is darker in the figure.
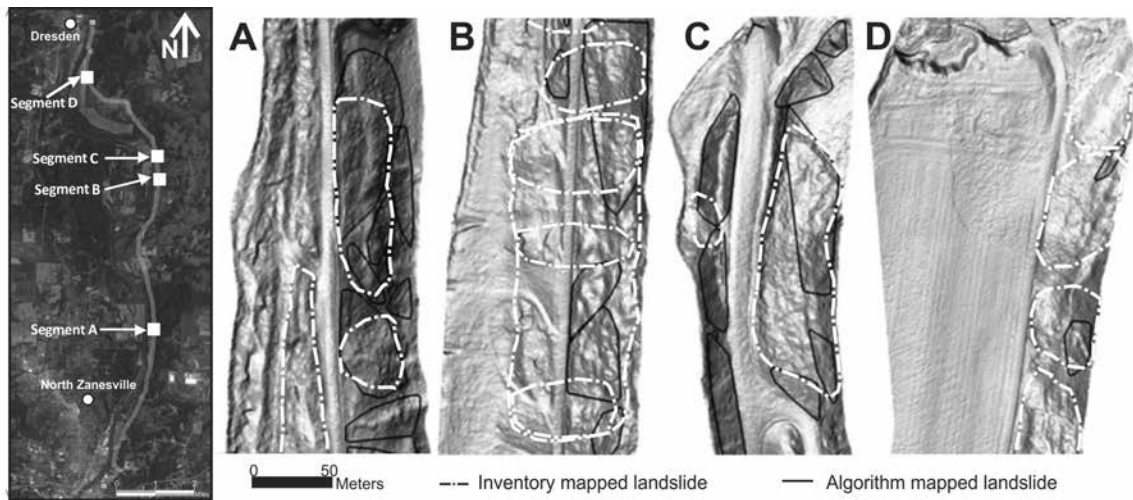

Figure 7. Comparison between the mapped landslide suspect areas by the proposed technique and those provided in the reference inventory map. The mapped landslides with a solid black line are those mapped by the proposed algorithm, and those mapped by the dashed line in white are the landslides mapped in the inventory map. The underlying DEM is a rasterized hillshade DEM.

landslides (reference), providing an accuracy of 55 percent for the algorithm. Additionally, twenty of the misclassified mapped areas were along rivers and creeks crossing the transportation network, which does not include areas along the Muskingum riverbank, thus, accounting for 10 percent of the mapped areas. The reason for these areas being consistently mapped can be attributed to the amount of erosion generated, in turn, creating high surface roughness. Nonetheless, the algorithm was able to identify 67 out of 80 mapped landslides in the inventory map, illustrating that 84 percent of the mapped landslides from the reference were identified. Although some of the mapped areas did not overlap the reference map, they were adjacent to these areas (see Figure 7C). Further analysis is necessary to verify that these mapped areas are indeed not new developing landslides or existing landslides that have developed further. Moreover, additional analysis is required to evaluate why some of the inventory mapped landslides were overlooked by the proposed algorithm. One reason for overlooking mapped landslides (reference) is the amount of surface roughness exhibited within the landslides (see SW corner of Figure 7A, West of road for Figure 7B and Figure 7D). The amount of surface roughness is not sufficient to delineate them from stable terrain. Therefore, these mapped landslides (reference) will go undetected, until enough surface roughness is displayed from experienced mass movement.

Conclusions

Landslide susceptibility mapping using remote-sensing techniques may never completely replace traditional mapping methods of field inspection, aerial photograph interpretation, and contour map analysis. Moreover, the mapping methods presented in this and other studies often rely on objective topographic data that relies on the morphologic expressions in the area studied, and often cannot differentiate between adjacent landslides. However, as the spatial resolution, accuracy, and availability of remote-sensing technology increases, new landslide susceptibility mapping methods will provide efficient tools that can assist traditional methods. The proposed approach quantifies and identifies landslide surface features producing results that can potentially become useful in the prevention of future hazardous events.

Although, the generation of landslide maps remains a subjective and time consuming task, airborne lidar provides new opportunities for mapping the topographic features found in small landslides. lidar technology has become both more accessible and affordable, and the advancements in airborne lidar have allowed for a new method to map landforms, including landslides, over broad swaths of terrain at higher spatial resolutions and accuracy. To our best knowledge, the literature has not capitalized on airborne lidar-derived DEMs to investigate small landslide susceptibility mapping at sub-meter scales over large

swaths of terrain under land cover. Previous landslide susceptibility mapping investigations have focused on geotechnical mapping evaluations over large landslides (e.g., Van Den Eeckhaut *et al.*, 2005; Booth *et al.*, 2009; Ballabio and Sterlacchini, 2012; Tien Bui *et al.*, 2012). Our study presents a new opportunity to map small failures utilizing airborne lidar-derived DEMs.

This proposed algorithm provides a means to evaluate each cell in the DEM to identify patterns of slope instability over the study area, which covers an area of approximately 3.0 square kilometers. The outputs of the algorithm were tested and compared to an independently compiled landslide inventory map to assess the classification performance. Assuming, that the landslide inventory is complete and accurate, our algorithm was able to identify 84 percent of the landslides in the study area. The findings of this study demonstrate that various types, scales, and deformations of landslide surface features (such as hummocky terrain, scarps and displaced blocks of material) can be extracted through the proposed approach and a surface model generated from sub-meter spatial resolution. Although, the local topographic roughness can be exploited through the geomorphological features described, an adequate sample representative of the study area is necessary to train the supervised classification algorithm. It is not foreseen for new landslide susceptibility mapping techniques to replace traditional mapping methods; however, new opportunities can improve the efficiency of landslide susceptibility mapping. Future studies may include; water tables or water entering the landslide area, the angle of internal friction of the landslide material and the configuration of the landslide itself.

In order to quantify the amount of activity observed between landslides, careful monitoring is necessary. It is clear that there are different scales and degrees of surface deformation observed within the landslides throughout the study site. To monitor and quantify the temporal changes, further research is necessary to investigate more quantitative patterns of the surface deformation observed, between the different landslides. However, this task is not time and cost-effective, although, it can be highly effective; it is dependent on the needs to monitor mass movement. The proposed approach allows for a semi-automated, fast, objective surface feature extraction of small landslide topography.

Acknowledgments

References

Ballabio, C., and S. Sterlacchini, 2012. Support vector machines for landslide susceptibility mapping: The Staffora River Basin case study, Italy, *Mathematical Geosciences*, 44(1):47–70.

Booth, A.M., J.J. Roering, and J.T. Perron, 2009. Automated landslide mapping using spectral analysis and high-resolution topographic data: Puget Sound lowlands, Washington, and Portland Hills, Oregon, *Geomorphology*, 109(3):132–147.

Galli, M., F. Ardizzone, M. Cardinali, F. Guzzetti, and P. Reichenbach, 2008. Comparing landslide inventory maps, *Geomorphology*, 94(3):268–289.

Glenn, N.F., D.R. Streutker, D.J. Chadwick, G.D. Thackray, and S.J. Dorsch, 2006. Analysis of lidar-derived topographic information for characterizing and differentiating landslide morphology and activity, *Geomorphology*, 73(1):131–148.

Gomez, H., and T. Kavzoglu, 2005. Assessment of shallow landslide susceptibility using artificial neural networks in Jabonosa River Basin, Venezuela, *Engineering Geology* 78(1):11–27.

Gonzalez, R.C., and R.E. Woods, 2002. *Digital Image Processing*, Addison-Wesley Longman Publishing Co., Inc., Boston, Massachusetts.

Guzzetti, F., A.C. Mondini, M. Cardinali, F. Fiorucci, M. Santangelo, and K.T. Chang, 2012.

Landslide inventory maps: New tools for an old problem, *Earth-Science Reviews*, 112(1):42–66.

Isenburg, M., 2013. LAStools - Efficient tools for lidar processing, URL: *http://www.cs.unc.edu/~isenburg/lastools/* (last date accessed: 12 January 2015).

Jaboyedoff, M., T. Oppikofer, A. Abellán, M.H. Derron, A. Loye, R. Metzger, and A. Pedrazzini, 2012. Use of LIDAR in landslide investigations: A review, *Natural Hazards*, 61(1):5–28.

James, L.A., M.E. Hodgson, S. Ghoshal, and M.M. Latiolais, 2012. Geomorphic change detection using historic maps and DEM differencing: The temporal dimension of geospatial analysis, *Geomorphology*, 137(1):181–198.

Kasai M., M. Ikeda, T. Asahina, and K. Fujisawa, 2009. LiDAR-derived DEM evaluation of deep-seated landslides in a steep and rocky region of Japan, *Geomorphology*, 113:57–69.

Katzil Y., and Y. Doytsher, 2003. A logarithmic and sub-pixel approach to shaded relief representation, *Computers & GeoSciences*, 29(9):1137–1142.

Micheletti, N., L. Foresti, M. Kanevski, A. Pedrazzini, and M. Jaboyedoff, 2011. *Landslide Susceptibility Mapping Using Adaptive Support Vector Machines and Feature Selection*, Master Thesis, University of Lausanne, Lausanne, Switzerland, 99 p.

Marjanovi , M., M. Kova evi , B. Bajat, and V. Voženílek, 2011. Landslide susceptibility assessment using SVM machine learning algorithm, *Engineering Geology*, 123(3):225–234.

McKean, J., and J. Roering, 2004. Objective landslide detection and surface morphology mapping using high-resolution airborne laser altimetry, *Geomorphology*, 57(3):331–351.

Samui, P., 2008. Slope stability analysis: A support vector machine approach, *Environmental Geology* 56(2):255–267.

Schwanghart, W., and N.J. Kuhn, 2010. TopoToolbox: A set of Matlab functions for topographic analysis, *Environmental Modelling & Software*, 25:770–781.

Shan, J., and C.K. Toth (editors), 2008. *Topographic Laser Ranging and Scanning: Principles and Processing*, CRC Press, Taylor and Francis Group.

Shapiro, L., and G. C. Stockman, 2001. *Computer Vision*, Prentice Hall, Englewood Cliffs, New Jersey.

Sherrod, P.H., 2008. *DTREG Predictive Modeling Software*, Users Manual, URL: *www.dtreg.com/DTREG.pdf* (last date accessed: 12 January 2015).

Soeters, R., and C.J. van Westen, 1996. Slope instability recognition, analysis and zonation, *Landslides, Investigation and Mitigation*, Transportation Research Board, National Research Council, Special Report, 247:129–177.

Steiger, J.R., 1996. *Soil Survey of Muskingum County, Ohio*, U.S. Department of Agriculture, Natural Resources Conservation Service.

Tien Bui, D., B. Pradhan, O. Lofman, and I. Revhaug, 2012. Landslide susceptibility assessment in Vietnam using Support vector machines, Decision tree and Naïve Bayes models, *Mathematical Problems in Engineering*.

Van Den Eeckhaut, M., J. Poesen, G. Verstraeten, V. Vanacker, J. Moeyersons, J. Nyssen, and L.P.H. van Beek, 2005, The effectiveness of hillshade maps and expert knowledge in mapping old deep-seated landslides, *Geomorphology*, 67:351–363.

Vapnik, V., 2000. *The Nature of Statistical Learning*, Springer, New York.

Wieczorek, G., 1984. Preparing a detailed landslide-inventory map for hazard evaluation and reduction, *Bulletin of the Association of Engineering Geologists*, 21(3):337–342.

Woodcock, N.H., 1977. Specification of fabric shapes using an eigenvalue method, *Geological Society of America Bulletin*, 88(9):1231–1236.

Yao, X., L.G. Tham, and F.C. Dai, 2008. Landslide susceptibility mapping based on support vector machine: A case study on natural slopes of Hong Kong, China, *Geomorphology*, 101(4):572–582.